Optical investigations of individual InAs quantum dots: Level splittings of exciton complexes

L. Landin, M.-E. Pistol,* C. Pryor, M. Persson, L. Samuelson, and M. Miller†
Department of Solid State Physics, Box 118, Lund University, S-221 00 Lund, Sweden
(Received 24 May 1999)

We have investigated individual InAs quantum dots embedded in GaAs using photoluminescence spectroscopy as a function of temperature and excitation power density. We also present $\mathbf{k}\cdot\mathbf{p}$ calculations including both direct and exchange interactions for systems with up to three excitons in the dot. From these calculations we are able to assign some of the many peaks observed to various few-particle states. A rate-equation model has also been developed which allows simulations of the peak intensities with excitation power density to be made and compared with experiment. [S0163-1829(99)04548-8]

I. INTRODUCTION

It has recently become possible to observe photoluminescence (PL) from individual quantum dots grown by the Stranski-Krastanov technique. This allows one to probe the electronic structure of a dot in the detail that will be required for a full understanding of these structures. The most widely studied system is InAs quantum dots embedded in GaAs barriers.[1] It has been observed that few-particle states are easily formed in such quantum dots,[2,3] as evidenced by the appearance of many closely spaced emission lines. The number of lines increases rapidly with increasing excitation power density, which is assumed to correlate with an increasing number of charge carriers in the dots.[2,3] At sufficiently low excitation power density, only single excitons (X) should be present, while higher excitation power density should produce biexcitons (X_2) and then triexcitons (X_3). In addition, charged states containing an extra electron or hole are also possible. Whatever excitons populate the dot, the PL spectrum will depend on the excitation power, due to interactions within the dot. Determining the nature of the dominant interactions (direct or exchange) and whether or not the excitons are neutral are central to unraveling the electronic structure of quantum dots.

In this paper we present high spectral resolution photoluminescence measurements of individual InAs quantum dots in GaAs. The experimental results are compared with $\mathbf{k}\cdot\mathbf{p}$ calculations that include direct and exchange interactions. In addition, a rate equation model is used to estimate the occupancy of the levels. Section II begins with an introduction to our notation for dealing with the complexities of multiparticle states in a quantum dot. Section III describes the sample growth, and the experimental arrangement for measuring the spectra. Section IV presents the PL spectra, and their dependence on excitation power density and temperature. Section V presents the results of our calculations of the electronic energy levels, and the transitions among them. Section VI discusses the relationship between the calculated levels and the observed peaks. Section VII presents our rate-equation model used to describe the occupancy of the levels, and presents a comparison with the results of the measurements.

II. MULTIPARTICLE STATES

It is extremely difficult to discuss multiexciton states without a clear notation. In spite of being referred to as ''artificial atoms,'' quantum dots have significantly less symmetry than an atom, making the customary atomic spectroscopic notation useless. Even if the dot possesses a discrete remnant of an atom's rotational symmetry, that symmetry may be difficult to determine, and may vary from system to system. The random nature of Stranski-Krastanov growth may even result in dots with no residual symmetry. Therefore, it behooves us to adopt a notation that is not tied to any assumed geometry of the dot, but rather deals directly with the filling of levels.

We specify states by the occupation numbers of the single electron and single hole orbitals. For example, $(e10{:}h02)$ is a state with one ground-state electron and two holes in the first excited orbital. For InAs/GaAs dots the typical spacing between single-particle energies is 10 meV for valence-band states, and 100 meV for conduction-band states. The Coulomb binding energy is on the order of 30 meV.[4] If the dot has no geometric symmetry each single-particle orbital is double degenerate due to the Kramer's degeneracy, making $(e10{:}h02)$ twofold degenerate. This degeneracy can be split by the exchange interaction, with typical spacings of a few meV or less in InAs/GaAs dots. Since the exchange splitting is much smaller than the contribution to the energy coming from the single-particle energies and the direct interaction, there is a clear separation of energy scales. Therefore it makes sense to refer to a state by its configuration of single-particle orbitals and its level within the exchange-split multiplet. We specify the states within an exchange-split multiplet by an additional subscript of the form s/t, where t is the total number of states in the multiplet and s identifies the states. For example, $(e10{:}h02)_{1/2}$ is the ground state of the $(e10{:}h02)$ configuration including the effect of exchange.

An additional complication arises if the dot is symmetric. In this case some single-particle orbitals will be more than twofold degenerate. This is indicated by a subscript on the integer giving the occupation number. For example $(e11_4{:}h20)_{1/8}$ is a four-particle state in which the conduction-band first excited state is fourfold degenerate, and contains one electron.

III. GROWTH AND MEASUREMENT

The dots were grown by chemical beam epitaxy, as described in Ref. 5. Atomic force micrographs show that the

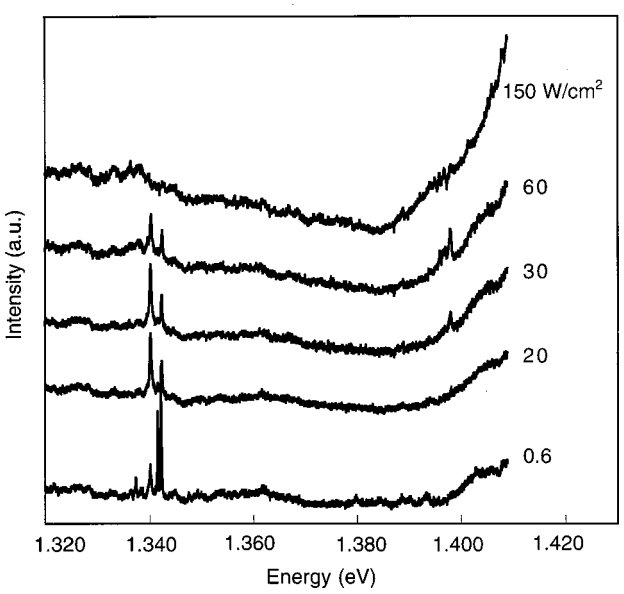

FIG. 1. Photoluminescence spectra of a single InAs quantum dot (QD1) for different excitation power densities. At low excitation power densities (<20 W/cm^2) only low-energy emission near 1.34 eV is seen. These transitions involve the ground-state single-particle orbitals. At higher excitation power density, emission appears near 1.40 eV, which involves configurations with excited single-particle orbitals. At the highest excitation power density (150 W/cm^2) the emission becomes broad and featureless.

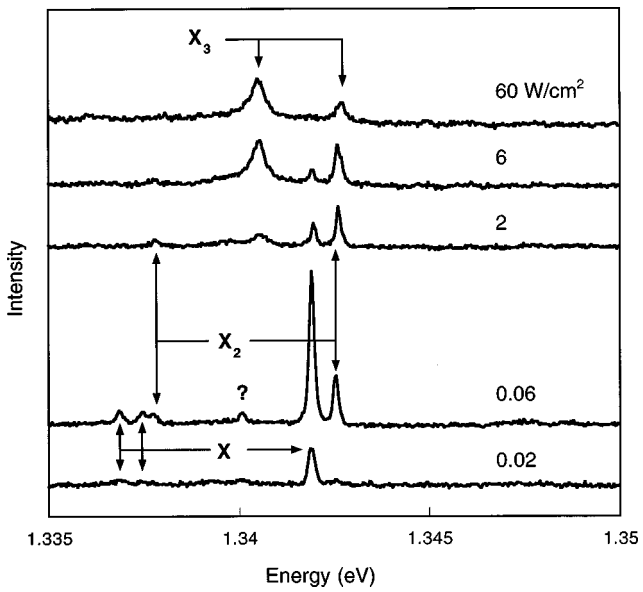

FIG. 2. Photoluminescence spectra of a single InAs quantum dot (QD1) for different excitation power densities. At the lowest excitation power density, three lines are seen, labeled X. At higher excitation power density two additional lines appear, labeled X_2. At still higher excitation power densities, new emission lines appear (X_3), and the original lines vanish. Groups of lines are labeled according to the exciton complex. There is also emission from an unknown state, indicated by a question mark.

dots have a typical height of about 4 nm, although there is considerable scatter. The lateral extension is less certain due to tip convolution, but we estimate about 10–12 nm. The dots are covered with a 20-nm GaAs capping layer and are thus fully strained.

PL measurements were performed in a flow cryostat designed for microphotoluminescence. The typical temperature was 5 K, as measured by a thermocouple in close proximity to the sample. No laser heating was observed, and this was checked by chopping the laser. The sample was lightly glued in one corner to avoid possible strain effects. For excitation we used a frequency-doubled yttrium aluminum garnet (YAG) laser emitting at 532 nm. Light was collected with a microscope, dispersed through a spectrometer, and then detected with a cooled charge-coupled device (CCD) camera. This technique, in combination with a low-density sample, produces PL spectra of individual dots.[2] Since we used a CCD camera for detection, no intermediate pinhole was used (as in confocal microscopy). The laser spot was typically 100 μm and a 20$\times$ objective with a long working distance was used. The integration times used were typically a few hours, with a maximum of 10 h. Usually two separate exposures were made, which allowed easy removal of noise spikes, and the exposures were then added in software. The excitation power density was adjusted with neutral density filters.

IV. EXCITATION POWER DENSITY AND TEMPERATURE DEPENDENCE

Ten dots were measured, all of which gave similar results. We will focus our attention on two of the dots, denoted QD1 and QD2. Figure 1 shows the emission spectra of QD1 for different excitation power densities, including the entire range from the lowest-energy transition to the low-energy tail of the wetting-layer emission. The observed lines fall into two distinct groups at low and high energy, around 1.34 and 1.4 eV, respectively. At the lowest excitation power density, the emission consists of a few low-energy peaks. At higher excitation power densities, some of the low-energy peaks vanish, while additional high-energy lines appear. At the highest excitation power the emission becomes broad and featureless. It has been proposed that this broadening is due to interactions with carriers in the wetting layer.[2]

Figure 2 is a detailed view of the low-energy emission spectrum for QD1 at different excitation power intensities. Groups of lines are labeled by the type of excitonic state to which we will ultimately ascribe the line. At the lowest excitation power density the emission consists of three lines. At increasing excitation power density new lines (X_2) appear 0.4 meV above and 4.0 meV below the strongest X line. Finally, at the highest excitation power density a third set of lines appears (X_3). The X_3 lines have a linewidth of about 0.3 meV which is significantly larger than the linewidths for X_2 and X (0.1 meV). The X_3 lines (presumably) arise from transition of the type $(e21{:}h21)\rightarrow(e11{:}h11)$. High-energy transitions of the type $(e21{:}h21)\rightarrow(e20{:}h20)$ also appear at high excitation power density (see Fig. 1).

Note that the strongest X line is at a lower energy than the strongest X_2 line. This is in disagreement with previous assignments.[6,7] However, those assignments were for experiments on dots of $In_xGa_{1-x}As$ in GaAs, and it appears that the energies are sensitive to the structure of the dots. Whether the recombination energy of a biexciton is above or below that of a single exciton is not straightforward to answer for a quantum dot. In a quantum well a biexciton is formed by a van der Waals–like attraction of excitons, mak-

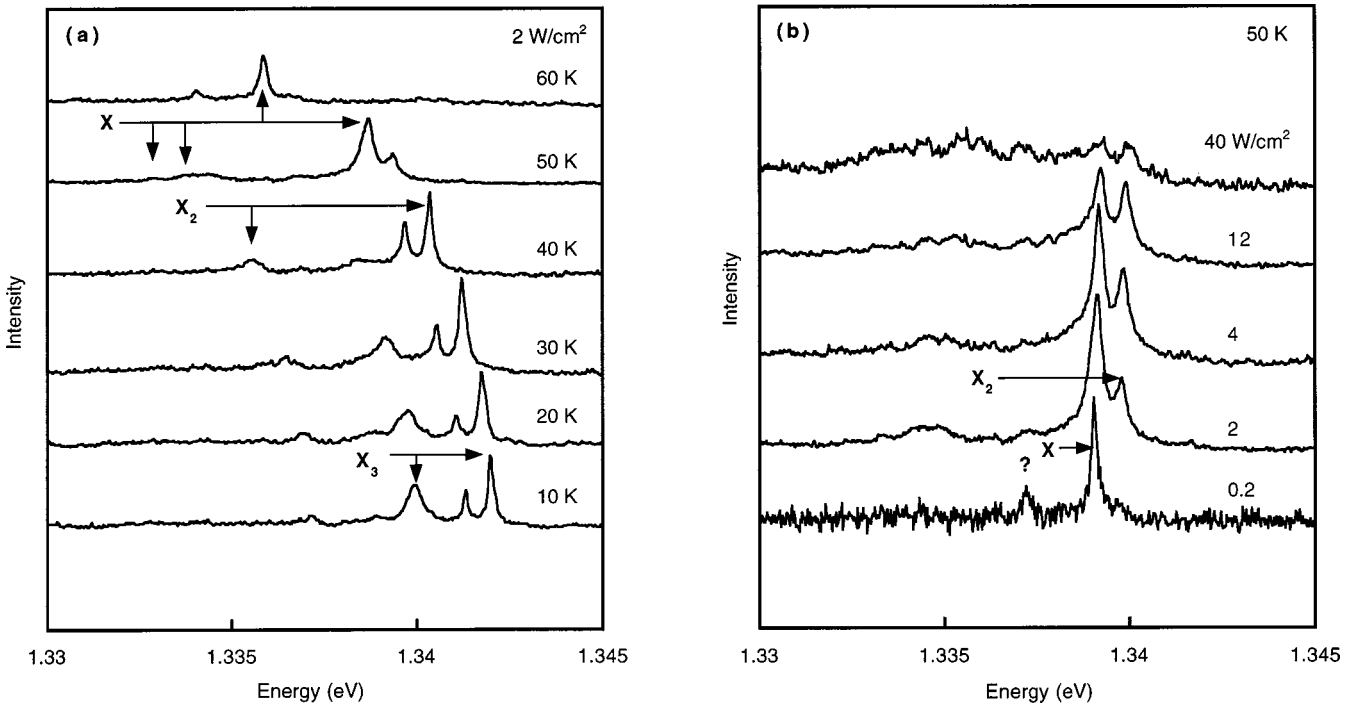

FIG. 3. (a) Evolution of the photoluminescence spectrum with temperature (QD1). At 10 K emission is seen from X, X_2, and X_3. At higher temperatures, the higher-order excitons quench. (b) Evolution of the photoluminescence spectrum with excitation power density at a temperature of 50 K. At the lowest excitation power only X is visible (in addition to the unknown line marked ?, which is the same line as in Fig. 2). At higher excitation power X_2 emission appears, but the X_3 emission never becomes visible.

ing the biexciton emission energy lower than that for a single exciton. In a quantum dot the situation is far more complex due to the strong confinement. The electron and hole wave functions are primarily determined by the strong confining dot potential. The Coulomb energy is determined by the charge distributions from these wave functions, and depends sensitively on the relative sizes of the electron-electron, hole-hole, and electron-hole interactions. By changing the dot structure, the charge densities, and thus the interactions, will be modified. It is therefore reasonable for the X and X_2 lines to be reversed in different dot structures. Such a phenomenon presents an interesting theoretical challenge; however, a more detailed characterization of the dot structure will be necessary.

Figure 3 shows the evolution of the QD1 spectrum with temperature. The excitation power density was chosen to allow the simultaneous observation of X, X_2, and X_3 lines. As the temperature increases X_3 quenches first, followed by X_2. At the highest temperature the emission is mostly from X. It is natural to assume that the triexciton should quench first, due to the presence of particles in excited orbitals with a corresponding low binding energy. This argument does not apply to the biexciton though, where all charge carriers are in their lowest orbitals. The quenching of the biexciton emission with temperature will be explained in Sec. V. If we increase the excitation power density, at a temperature of 50 K we never observe the triexciton, as shown in Fig. 3, indicating that the thermal emission rate is faster than the emission rate for this state at this temperature. We do, however, recover the biexciton emission at higher excitation power density.

At low excitation power density there is a mystery line for which we do not have an assignment. This line has an intensity that decreases with excitation power density more rapidly than the X lines. This indicates that this line is not related to X, and it may be due to a charged exciton.

In Fig. 4 we show the emission spectrum of QD2 for different excitation power densities. The behavior is very similar to QD1, and we can follow the emission from X, X_2, and X_3. Emission lines from $(e1{:}h1)_{1,2/4}$ were not observed in this dot, despite a 10 h integration time. In Fig. 4 we also show the evolution with temperature of the emission from QD2, at an excitation power density where emission from X, X_2, and X_3 is simultaneously observed. The same behavior as for QD1 is observed with X_3 quenching first, followed by X_2 and finally X. What is generally true for all measured dots is that the highest-energy emission line of X_2 appears at a higher energy than the highest-energy emission line of X. The energy difference between the X_3 emission lines and the X_2 emission lines is not as consistent from dot to dot as that between X and X_2.

V. ELECTRONIC STRUCTURE CALCULATIONS

Energy levels and wave functions were calculated using a $\mathbf{k}\cdot\mathbf{p}$ model, including Coulomb charging effects, and the exchange interaction. The strain distribution was computed using the finite element method, and then used in a strain-dependent eight-band $\mathbf{k}\cdot\mathbf{p}$ Hamiltonian to compute the single-electron and single-hole wave functions. Details of the method used to calculate single-particle states and the relevant material parameters may be found elsewhere.[4]

The single-particle wave functions were then used to construct a multiparticle basis in which the direct and exchange Coulomb interaction Hamiltonian were diagonalized. The single-particle wave functions come as degenerate pairs, re-

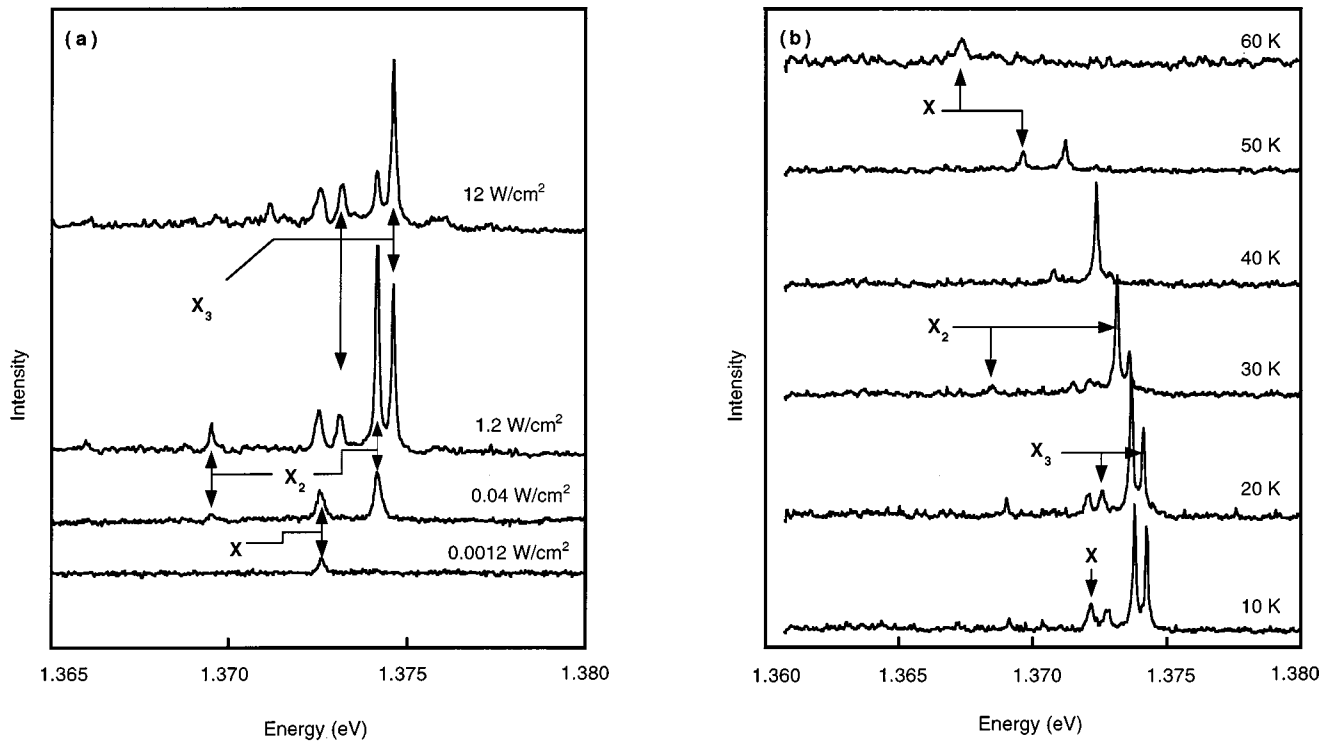

FIG. 4. Photoluminescence spectra of a single dot (QD2). The evolution of the spectra with excitation power density and temperature is very similar to that of QD1, shown in Figs. 2 and 3.

lated to each other by time reversal. Thus, for a noninteracting system each single-particle energy level may contain two particles. This is still true if direct interactions are included, since the direction interactions depend only on the charge density. The exchange interaction is considerably more complex since it involves the spinor structure of the multiband wave function.

The exchange interaction is divided into short- and long-range pieces. We will consider the dominant short-range component given by $H_{sr}=\alpha\vec{\sigma}\cdot\vec{J}$ where $\vec{\sigma}$ is the spin-$\frac{1}{2}$ operator acting on the Γ_6 components of the conduction band, $\vec{J}$ is the spin-$\frac{3}{2}$ operator acting on the Γ_8 components of the valence band, and α is a material-dependent constant. Since α depends on the microscopic details of the wave function, it is fit to experimental data. In our case, α was fit to experiments on InAs nanocrystals.[8]

Multiparticle states were found by first choosing which of the single-particle energy levels were filled with electrons and holes. The multiparticle wave function was then taken to be a linear combination of all possible combinations of filled orbitals. For example, consider a single exciton in the $(e10{:}h10)$ configuration. Let $\phi_e(x)$ and $\phi_h(x)$ be the single-electron and single-hole ground-state wave functions. These are each degenerate with their time reverses, $T\phi_e(x)$ and $T\phi_h(x)$. The exciton wave function is taken to be of the form

$$a\phi_e(x_e)\phi_h(x_h)+bT\phi_e(x_e)\phi_h(x_h)+c\phi_e(x_e)T\phi_h(x_h)+dT\phi_e(x_e)T\phi_h(x_h). \quad (1)$$

In this basis, the Hamiltonian for the direct and exchange interactions is a 4×4 matrix, which is easily diagonalized once its matrix elements have been calculated from the ϕ's. Optical transitions were calculated in the dipole approximation. For multiexcitons there are some important technical details concerning the overlaps between the initial and final states of the nonrecombining particles. Further details of the calculations are available elsewhere.

The geometry of the dot was assumed to be a square-based pyramid with 101-type sides. The height was varied between 4.1 and 4.7 nm, which corresponds to a base length ranging from 5.8 to 6.6 nm. This size was chosen to give a lowest transition energy which agrees with the experiments.

Calculations were done for up to three excitons in the dot. Figure 5 shows the energy levels for a dot with a 6.6-nm base. The most important feature is that the ground-state single exciton which is fourfold degenerate in the absence of exchange, is exchange split into four states. The states are found in two groups of closely spaced doublets, with 0.18 meV between $(e1{:}h1)_{1/4}$ and $(e1{:}h1)_{2/4}$, and 0.1 meV between $(e1{:}h1)_{3/4}$ and $(e1{:}h1)_{4/4}$. The doublets are separated from each other by 3.8 meV. From the dipole matrix elements we find that the ground state $(e1{:}h1)_{1/4}$ is dark, while $(e1{:}h1)_{2/4}$ is extremely dim ($<10^{-3}$ of a typical allowed transition). The two states of the upper doublet are optically active. In spite of their dipole suppression, the two lower states may still be observable due to phonon interaction; however, they would be expected to be significantly dimmer.

Transitions involving X_2 reflect the same pattern as seen in X. However, the role of exciton relaxation is different because the quadruplet of $(e1{:}h1)$ states are now the final state. Even if excitons were to relax instantaneously to their ground state, the transition $X_2\rightarrow X_1$ would involve all four $(e1{:}h1)$ states.

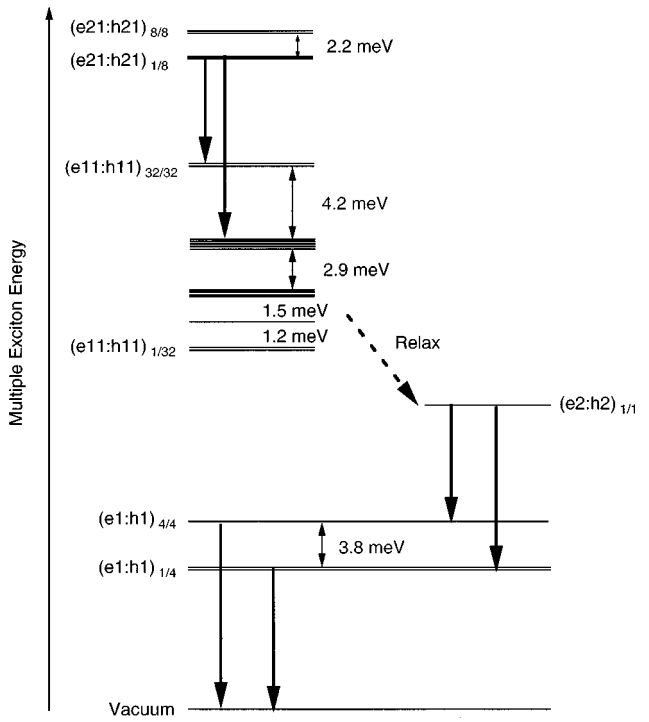

FIG. 5. Level structure for an InAs quantum dot with up to three excitons. The notation is explained in Sec. II of the text. The main radiative transitions observed experimentally are indicated by full arrows. Additional transitions that are not directly observed in experiments are denoted by dashed arrows.

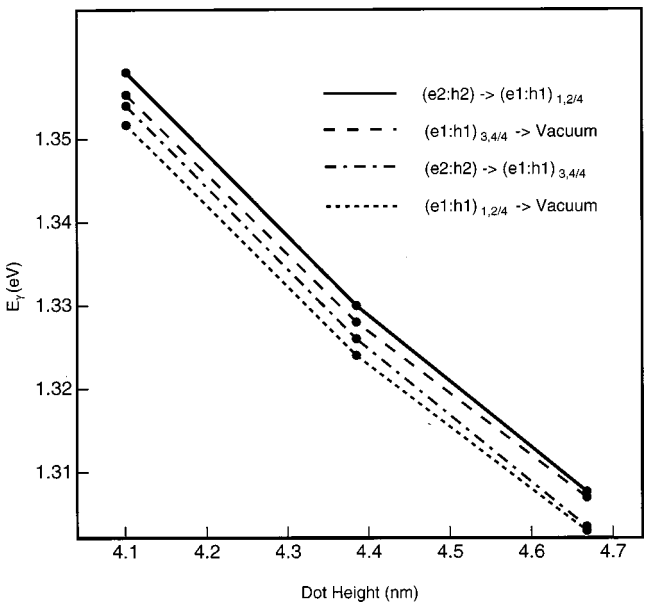

FIG. 6. Calculated transition energies for X and X_2 as a function of dot height, where the shape of the dot was kept fixed.

For X_3 the situation is even more complex. Because $(e11{:}h11)_{1-32/32}$ are possible final states, there are 32 possible transitions involving $(e21{:}h21)_{1/8}$ as the initial state, although only 16 of them are dipole allowed. The $(e11{:}h11)$ states appear in clusters of levels with spacings of less than 1 meV, with spacings of a few meV between the clusters. Hence, the $(e21{:}h21)\rightarrow(e11{:}h11)$ transitions would be expected to be seen as broad lines separated by a few meV.

The details of the spectrum can change significantly with dot geometry, although the qualitative features remain unchanged. Figure 6 shows the effect of island size on the $e1{:}h1\rightarrow$vacuum transition. The span of the multiplet is relatively insensitive to size over the limited range considered. The spacings within the multiplet are more sensitive to island geometry.

VI. PEAK ASSIGNMENTS

We now turn to assigning the observed PL peaks to the transitions we have calculated. This is a challenging task since the island shape and size can have a strong influence on the pattern of spacings, but the precise size and shape of an individual dot is uncertain. Considering the power-dependent spectra of Fig. 2, we see that the three PL peaks observed at the lowest excitation power consist of two low-energy peaks 0.6-meV apart, and another peak 4.0-meV higher. The two low-energy peaks are extremely small, in agreement with the calculations predicting one dipole-forbidden state and a dim state. The spacings also agree with the calculations. However, only a single high-energy peak is observed instead of the predicted doublet. We believe this single high-energy peak is in fact an unresolved doublet. Note that a charged exciton $(e2{:}h1)$ or $(e1{:}h2)$ has only one doubly degenerate state, producing only a single emission line. Hence, we cannot assign such configurations to the emission lines labeled X in Fig. 2.

The $(e2{:}h2)$ configuration consists of only one state. Consequently the $(e2{:}h2)\rightarrow(e1{:}h1)$ transitions must have the same spacing as the $(e1{:}h1)\rightarrow$*vacuum* transitions (in the first case because of the unique initial state and in the latter case because of the unique final state). This is exactly what we observe within the precision of our experiments, although one possible line is not observed. The relevant transitions are marked X_2 in Fig. 2.

The $(e21{:}h21)$ configuration has eight states and the relevant final configuration, $(e11{:}h11)$, has 32 states. We would thus expect 256 possible emission lines from the $(e21{:}h21)\rightarrow(e11{:}h11)$ transition. The calculations show that about half of these lines should be optically active. In our experiments we only observe two lines, denoted X_3 in Fig. 2. The energy position and splittings of these lines are consistent with the $(e21{:}h21)_{1-6/8}\rightarrow(e11{:}h11)_{23-30/32}$ transitions giving rise to the highest energy peak and the $(e21{:}h21)_{1-6/8}\rightarrow(e11{:}h11)_{31-32/32}$ transitions giving rise to the lowest energy peak. If we assume that all states within 0.5 meV of the ground state of the triexciton are populated, i.e., the $(e21{:}h21)_{1-6/8}$ states, we calculate the spectrum shown in Fig. 7. In the figure we also show the energy position of the highest emission lines of X_2 (which are closely spaced). As can be seen from the calculation the emission lines appear in groups, which explains the experimental fact that the linewidth of the X_3 emission is significantly larger than for the X and X_2 emission lines (see Fig. 2). Our assignment of the X_3 emission lines is mostly based on the energy position and is thus quite uncertain. In order to make a more reliable assignment, it is necessary to determine the occupation of the states in the initial configuration. The situation could be clarified by selective excitation experiments.

The mystery line in Figs. 2 and 3(b) remains unassigned.

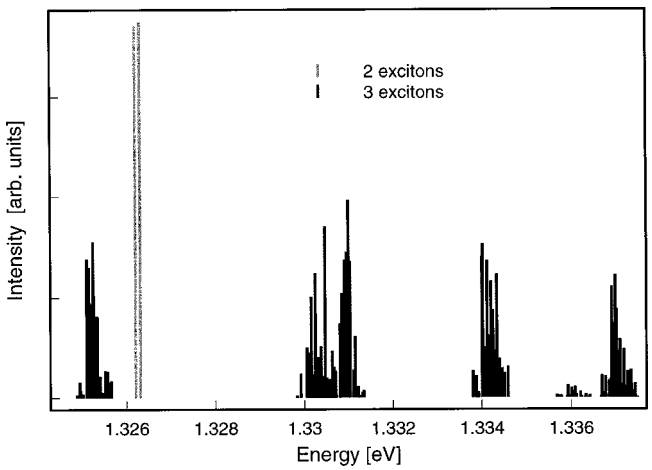

FIG. 7. Calculated spectra of an InAs quantum dot containing an X_3 that recombines to produce X_2. The energy for X_2 recombination is also indicated. Only the two emission lines with the highest energy are shown for the X_2 emission.

It is tempting to assume that this line is related to the biexciton and that the triexciton is responsible for the lines marked X_2. We do not favor such an interpretation, since the mystery line does not increase in intensity relative to the exciton for increasing excitation power density, as can be seen in Fig. 3(b). This intensity behavior has been observed also in other dots. The most likely explanation, is that this line is due to a charged exciton (which should have only one emission line). Although we believe our assignment of the peaks is the most likely we note that there are many difficulties, both experimental and theoretical. We do not know the shape of the dots very accurately and we do not know the degree of intermixing, making the calculations somewhat unreliable. There is also a possibility that there are additional lines that are below our detection limit.

VII. RATE EQUATIONS

The observed intensities depend on the occupations of the various levels. The occupations depend on the excitation power, the transition probabilities, and the temperature. We have developed a general rate-equation model in order to simulate some of our experimental results and to provide a consistency check on our assignments. The situation is slightly different from the rate equations used in atomic physics since the objects of interest are electron-hole pairs. Consider a dot in which one exciton is present. This exciton can be removed in two ways, either by recombination or by capturing an additional exciton to form a biexciton.

If we assume that each configuration consists of only one state we get

$$\frac{\partial N_1}{\partial t}=N_{ex}\omega_c\left(1-\sum_{k=1}^{n}N_k\right)+\omega_{2,1}N_2-\omega_{1,0}N_1-N_{ex}\omega_c N_1,$$

$$\frac{\partial N_k}{\partial t}=N_{ex}\omega_c N_{k-1}+\omega_{(k+1),k}N_{k+1}-\omega_{k,(k-1)}N_k-N_{ex}\omega_c N_k,$$

$$\frac{\partial N_n}{\partial t}=N_{ex}\omega_c N_{n-1}-\omega_{n,n-1}N_n, \tag{2}$$

where N_{ex} is the number of electron-hole pairs in the bulk (which is proportional to the excitation power density), N_k is the occupation probability of configuration k (i.e., X_k), $\omega_{k,(k-1)}$ is the recombination probability for $X_k \rightarrow X_{k-1}$, ω_c is the capture probability, and n is the maximum number of excitons that can be bound to the dot. The factor $(1-\Sigma_{k=1}^{n}N_k)$ in the first equation ensures probability conservation and could also be labeled N_0 (a dot without carriers) resulting in the constraint $\Sigma_{k=1}^{n}N_k=1$.

In reality each configuration has several states among which transitions also may occur. This modifies each equation in (1) to

$$\frac{\partial N_k^{\alpha}}{\partial t}=N_{ex}\frac{\omega_c}{M_k}\sum_i N_{k-1}^{i}+\sum_i \omega_{k+1,k}^{i,\alpha}N_{k+1}^{i}-\sum_i \omega_{k,k-1}^{\alpha,i}N_{k+1}^{\alpha}$$

$$-N_{ex}\omega_c N_k^{\alpha}+\sum_{i\neq\alpha}\omega_{k,k}^{i,\alpha}N_k^{i}-\sum_{i\neq\alpha}\omega_{k,k}^{\alpha,i}N_k^{\alpha} \tag{3}$$

and the sum in $(1-\Sigma_{k=1}^{n}N_k)$ must be replaced by $(1-\Sigma_{k=1,\alpha}^{n}N_k^{\alpha})$ to include each state in the configuration. The subscript in N_k^{α} identifies the configuration and the superscript the particular state. $\omega_{k+1,k}^{i,\alpha}$ is the probability of transitions from state N_{k+1}^{i} to state N_k^{α}, and M_k is the number of states within configuration X_k. Even more general models may be constructed, such as including thermal dissociation of excitons, but already at this stage there are many unknown parameters.

We have numerically solved the system of rate equations using a few simplifying assumptions in order to minimize the number of unknown parameters. We assume that the recombination probabilities of X_2 and X_3 are the same and that the capture probabilities of X, X_2, and X_3 are all equal and fast. For the recombination probability of X we use the calculated values (see Sec. IV). For transition between states in a configuration with two levels (labeled 1 and 2 with 2 highest in energy) we use the following probabilities, which are compatible with thermodynamics:[9]

$$\omega_{k,k}^{1,2}=\frac{\gamma}{e^{\Delta E/kT}-1},$$

$$\omega_{k,k}^{2,1}=\frac{\gamma}{e^{\Delta E/kT}-1}+\gamma, \tag{4}$$

where ΔE is the energy difference between the two different states in the configuration and γ is a rate which is a fitting parameter and is a measure how quickly the states will thermalize. Equation (4) may be generalized if more levels are involved.[9] With these assumptions we are left with two free parameters for excitation power density sufficiently low that only X_1 and X_2 are populated.

In the first calculation, we have calculated the ratio of the population probability of X and X_2 (i.e., N_1/N_2) as a function of excitation power density. The result is shown in Fig. 8 along with experimental data. We use the ratio of the population probabilities, since this is less sensitive to experimental errors than the absolute population probabilities. We find that the model explains the data quite well. In the inset of Fig. 8 we also show the calculated population probabilities of X, X_2, and X_3 as a function of excitation power density.

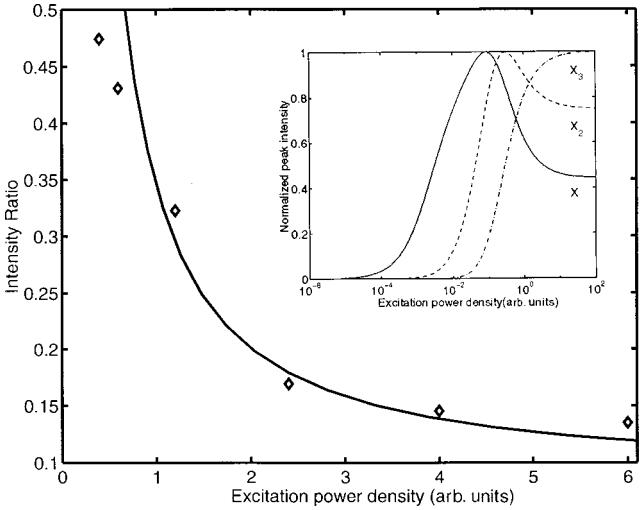

FIG. 8. A plot of the calculated intensity ratio of X and X_2 as a function of excitation power density along with experimental data. The inset shows the normalized intensities of X, X_2, and X_3 as a function of excitation power density.

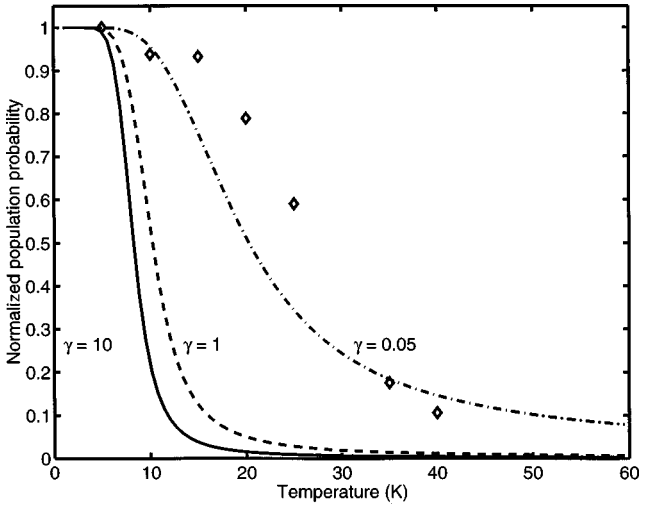

FIG. 9. A plot of the calculated intensity of X_2 as a function of temperature for different values of the thermal rate constant γ. The recombination probability of X has been set to one. The best fit is obtained with a low thermalization rate, about 20 times lower than the recombination rate.

Due to the many states involved when triexcitons are populated there are many unknown parameters and the result is quite qualitative. We note that for certain excitation power densities, there should be emission from X, X_2, and X_3, in agreement with our experimental results.

In Figure 9 we plot the calculated intensities of X_2 as a function of temperature, along with the experimental data. The excitation power density was chosen to make N_1 and N_2 comparable at $T=5$ K. As the temperature is increased, X_2 quenches rather quickly, in agreement with experiment. The physical reason is that at low temperature, X is primarily in its lowest states, $(e1{:}h1)_{1,2/4}$, which has a low recombination probability, and a biexciton is easily formed. At higher temperatures, however, X will be excited to $(e1{:}h1)_{3,4/4}$ which has a high recombination probability and it will thus be harder to form a biexciton. The fact that our rate-equation model agrees with the measured intensities supports our peak assignment.

We find that the rate of thermalization is about 20 times slower than the recombination rate of $(e1{:}h1)_{3,4/4}$ (i.e., using γ as a fitting parameter). This is a robust prediction of the simulations.

VIII. SUMMARY

In summary, we have in some detail investigated individual InAs quantum dots in GaAs both by experimental and theoretical means. By comparing experiment and theory we have made an assignment of the different emission lines to various transitions between multiparticle states.

ACKNOWLEDGMENTS

This work was performed within the Nanometer Structure Consortium in Lund and was supported by grants from the Swedish Natural Science Research Council (NFR), the Swedish National Board for Technical Development (NUTEK), the Swedish Research Council for Engineering Sciences (TFR), and the Swedish Foundation for Strategic Research (SSF).

*Author to whom correspondence should be addressed. Electronic address: mats-erik.pistol@ftf.lth.se

†Present address: Department of Electrical Engineering, University of Virginia, Charlottesville, Virginia, 22903.

[1] D. Leonard, M. Krishnamurthy, C. M. Reaves, S. P. DenBaars, and P. M. Petroff, Appl. Phys. Lett. **63**, 3203 (1993).

[2] L. Landin, M. S. Miller, M.-E. Pistol, C. Pryor, and L. Samuelson, Science **280**, 262 (1998).

[3] E. Dekel, D. Gershoni, E. Ehrenfreund, D. Spektor, J. M. Garcia, and P. M. Petroff, Phys. Rev. Lett. **80**, 4991 (1998).

[4] C. Pryor, Phys. Rev. B **57**, 7190 (1998).

[5] S. Jeppesen, M. S. Miller, D. Hessman, B. Kowalski, I. Maximov, and L. Samuelson, Appl. Phys. Lett. **68**, 2228 (1996).

[6] H. Kamada, H. Ando, J. Temmyo, and T. Tamamura, Phys. Rev. B **58**, 16 243 (1998).

[7] A. Kuther, M. Bayer, A. Forchel, A. Gorbunov, B. B. Timofeev, F. Schäfer, and J. P. Reithmaier, Phys. Rev. B **58**, R7508 (1998).

[8] U. Banin, J. C. Lee, A. A. Guzelian, A. V. Kadavanich, and A. P. Alivisatos, J. Cryst. Growth **22**, 559 (1997).

[9] A. E. Siegman, *Lasers* (University Science Books, Mill Valley, CA, 1986).